



Full length article



# Activation–Relaxation Technique: An efficient way to find minima and saddle points of potential energy surfaces

Antoine Jay<sup>a</sup>, Miha Gunde<sup>a</sup>, Nicolas Salles<sup>b</sup>, Matic Poberžnik<sup>b</sup>, Layla Martin-Samos<sup>b</sup>,  
Nicolas Richard<sup>c</sup>, Stefano de Gironcoli<sup>b</sup>, Normand Mousseau<sup>d,\*</sup>, Anne Hémerlyck<sup>a</sup>

<sup>a</sup> LAAS-CNRS, Université de Toulouse, CNRS, Toulouse, France

<sup>b</sup> CNR-IOM, Democritos and Sissa, Trieste, Italy

<sup>c</sup> CEA, DAM, DIF, F-91297 Arpajon, France

<sup>d</sup> Département de physique and Regroupement québécois sur les matériaux de pointe, Université de Montréal, case postale Centre-ville, Montréal (Québec), Canada, H3C 3H7

## ARTICLE INFO

### Keywords:

Activation–Relaxation Technique  
Activated mechanisms  
Atomistic modelling  
Saddle-point search  
Catalysis reactions  
Atomistic diffusion

## ABSTRACT

The Activation–Relaxation Technique (ARTn) is an efficient technique for finding the minima and saddle points of multidimensional functions such as the potential energy surface of atomic systems in chemistry. In this work we detail and illustrate significant improvements made to the algorithm, regarding both preprocessing and the activation process itself. As showcased, these advances significantly reduce ARTn computational costs, especially when applied with *ab initio* description. With these modifications, ARTn establishes itself as a very efficient method for exploring the energy landscape and chemical reactions associated with complex mechanisms.

## 1. Introduction

Understanding molecular reactions and the evolution of atomic structures is of crucial interest in modern chemistry and materials science. This objective requires a precise knowledge of the energy landscape associated with diffusion pathways, including the initial, final and transition states, as well as their relative free energies, *i.e.*, barrier energy and entropy.

Mathematically, for purely activated events in which energy barriers are high compared to temperature, the initial and final states can be assigned to a local energy minimum on the potential energy surface (PES) of the system, whereas the transition states are assigned to a first-order saddle point, corresponding to the highest energy point on the minimum-energy path connecting these two minima. Once these states are known, the kinetics of the system can be described within the framework of the transition state theory [1,2]. The reader should refer to the Appendix A for a better understanding of some key words used in this work.

The challenge to identify these states is two-fold: first, finding local points of interest; second, sampling the landscape to ensure that all the relevant mechanisms are identified. For a chemical system composed of  $N_{at}$  atoms, the PES has  $3N_{at}$  dimensions. While a local minimum of this PES can be easily reached by any algorithm that follows the slope in all these dimensions, saddle points are unstable along one

particular dimension called the valley, and are therefore harder to identify. Indeed, reaching a saddle point implies a relaxation in the  $3N_{at} - 1$  other dimensions and a climb along this unknown dimension of negative curvature. The curvature is, by definition, positive around a local minimum and does not provide information concerning the nature and position of saddle points sitting on the ridge between two minima. Such information can become available only beyond the inflection line surrounding a minimum: above this line, the valleys leading to these saddle points start to form and to dissociate (see the shoulders area in Fig. A.7(c) of Appendix A). For all these reasons, identifying local transition states remains a formidable task.

The Activation Relaxation Technique nouveau (ARTn) [3,4] has demonstrated to be a very efficient and versatile approach for finding saddle points on a PES using only local information (energy and forces). Doing so, it addresses both challenges underlined in the previous paragraph: the identification of local saddle point as well as, through its unbiased search approach, the capacity to provide an extensive mapping of the PES through fully connected activated paths. Over the last 20 years, ARTn has been applied to a wide range of systems both to explore their energy landscape [5–9], and to generate long-time kinetic trajectories [10–15] when used as kinetic ART, an off-lattice kinetic Monte Carlo algorithm with on-the-fly cataloguing. When searching for a saddle point, a recent implementation of ARTn coupled with

\* Corresponding author.

E-mail addresses: [ajay@laas.fr](mailto:ajay@laas.fr) (A. Jay), [normand.mousseau@umontreal.ca](mailto:normand.mousseau@umontreal.ca) (N. Mousseau), [anne.hemeryck@laas.fr](mailto:anne.hemeryck@laas.fr) (A. Hémerlyck).

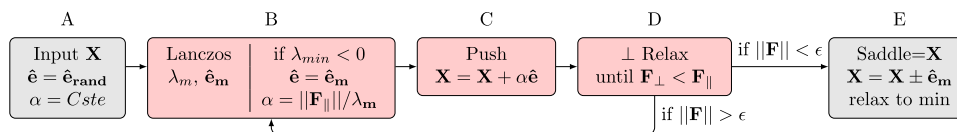


**Fig. 1.** The three main steps of ARTn (in pink) that find a saddle point from an initial input position  $X$ , a given random vector  $\hat{e}_{rand}$ , and a norm  $\alpha$  for this random push. The lowest eigenvalue  $\lambda_m$  ( $m$  as minimum) of the Hessian matrix and its corresponding eigenvector  $\hat{e}_m$  are calculated with the Lanczos procedure.  $\mathbf{F}_\perp = (\mathbf{F} \cdot \hat{e})\hat{e}$  is the component of the forces  $\mathbf{F}$  that is parallel to the pushing direction  $\hat{e}$  and  $\mathbf{F}_\parallel = \mathbf{F} - \mathbf{F}_\perp$  is the orthogonal component.

Density Functional Theory (DFT) (ARTn-DFT in the following) [16], was shown to result in more accurate saddle points — *i.e.* with total force many orders of magnitude lower — and to be computationally less expensive than the climbing image-nudged elastic band (NEB) method [17]. Previous work has also shown that ARTn is more efficient than the dimer method [18] for generating a fully connected PES with multiple saddle points search [19].

The scope of this work is to present an overview of the ARTn method and the latest improvements on the core algorithm as well as pre-processing strategies when running multiple-saddle-point search. These improvements further reduce the number of energy and force evaluations while keeping whole numerical accuracy. The basic structural elements of ARTn are outlined in Section 2, while latest improvements and pre-processing strategies are discussed in Sections 3 and 4, respectively.

## 2. Standard Activation Relaxation Technique nouveau

The core of ARTn is based on three stages that are executed at every step of the search until convergence is achieved:

- Evaluation of the Hessian lowest eigenvalue  $\lambda_m$  (lowest curvature), *i.e.* the one with the most negative value, or with the smallest value if they are all positive and its corresponding eigenvector  $\hat{e}_m$  (direction along which the curvature is the lowest);
- Uphill push, against the forces;
- Relaxation into the hyperplane perpendicular to the push.

This workflow is shown in Fig. 1 (pink blocks). The choice of the initial push (first grey block in Fig. 1) and the possibility for searching multiple-saddle points are, here, considered as pre-processing and post-processing operations, respectively. Fig. 2(a) illustrates ARTn searches on a bi-dimensional (2D) potential energy surface model.

The concept of the algorithm is simple. In practice, however, its performances (reduced number of energy and force evaluations, numerical stability, success rate and precision) rely on several numerical and mathematical tricks.

In this section we discuss a few central elements of ARTn.

### 2.1. Initial uphill push

Since a local energy minimum does not provide information regarding the position or nature of the saddle points connected to it, by default, ARTn generates a random push ( $\hat{e}_{rand}$ ) from a local minimum to start an event search.

In the absence of strong mathematical justification, many approaches can be used for this initial deformation: the random displacement can be applied to a single atom, a local environment, or to the entire system dimensions. Since, irrespective of the number of atoms involved in the initial displacement, ARTn imposes no constraints on the atoms that can move, all saddle points can, in principle, be found, regardless of the initial push. In practice, however, “smart” choices of the initial push improve the sampling of the saddle point. For example, global pushes tend to oversample collective transition states often related to soft degree of freedom. On the contrary, very local pushes tend to sample transition states that only involve the breaking or formation

of few bonds (hard degree of freedom). Since activated events away from phase transitions tend to be local in nature, typical initial random deformation are therefore applied on local environments counting a limited number of atoms.

While there is no formal proof that ARTn can generate an exhaustive list of activation barriers connected to a local minimum, the random search permits to limit the biases. In fact, it has been shown that a sufficient number of random explorations generates a larger catalogue of events than competing algorithms, while always retrieving previously known barriers [4,12,20].

### 2.2. Evaluation of the lowest curvature

During this stage, the lowest eigenvalue ( $\lambda_m$ ) and corresponding eigenvector ( $\hat{e}_m$ ) of the Hessian matrix are evaluated by means of Lanczos algorithm [21] (see Appendix B). This lowest eigenvalue determines if the system is below ( $\lambda_m > 0$ ), or above the inflection hyperplane ( $\lambda_m < 0$ ). Once above this hyperplane, the initial uphill push direction is switched to  $\hat{e}_m$ . To reduce the computational cost, in practice, if ARTn search starts in a minimum, the lowest curvature could be computed only after few uphill pushes as the curvature is positive near a minimum, by definition.

### 2.3. Uphill push

The uphill push is performed to (i) escape from the harmonic basin surrounding the minimum and (ii) to move towards a ridge. The push direction depends on the position of ARTn on the PES:

1. Below the inflection hyperplane, *i.e.*, where are directions have positive curvature, the push direction is kept constant and equal to the initially chosen direction.
2. Above the inflection, *i.e.*, where the lowest curvature  $\lambda_m$  is negative, with absolute value larger than a given threshold  $\lambda_{thr}$ , the push direction is updated to the corresponding eigenvector  $\hat{e}_m$  with an orientation set opposite to the force and the norm of the displacement set as in Ref. [22]:

$$dr = \min \left( size_{max}, \frac{\|\mathbf{F}_\parallel\|}{\max(|\lambda_{min}|, 0.5)} \right), \quad (1)$$

where  $\mathbf{F}_\parallel$  is the component of the force that is parallel to  $\hat{e}_{min}$  and  $size_{max}$  is a user defined threshold. This adaptive norm reduces the size of the displacement when the system is close to the saddle point and was shown to accelerate convergence.

### 2.4. Orthogonal relaxation

To reach convergence to a first-order saddle, the  $3N_{at} - 1$  directions orthogonal to  $\hat{e}_m$  must be in a local minimum. As for the uphill push, this orthogonal relaxation plays two different roles depending on whether the system is below or above the inflection plane.

1. Below the inflection, a weak orthogonal relaxation is applied to avoid too short interatomic distances that could result from the application of the uphill push. A small number of relaxation steps is then sufficient to assure stability, whereas a whole

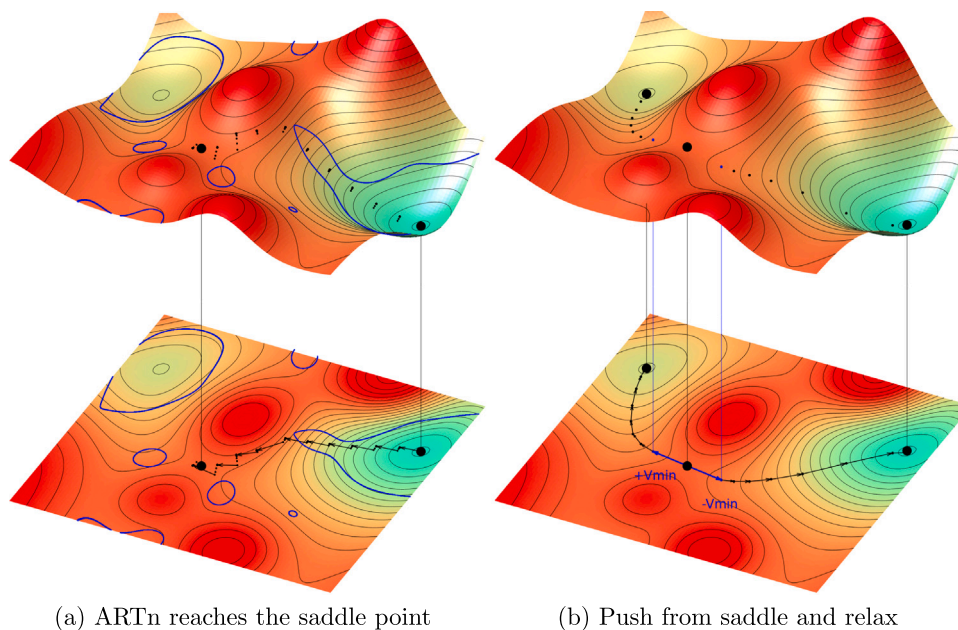


**Fig. 2.** A complete event generated with ARTn on a two-dimensional potential energy surface. **2(a)** An ARTn event is launched from a local energy minimum. Each black dot is an ARTn step. The black arrows are the pushing directions at each step. The first steps, below the inflection line defined by all the point for which the lowest eigenvalue  $\lambda_m$  is zero (in blue), are pushes in a predetermined random direction followed, at each step, by a slight perpendicular relaxation to avoid collisions. Above the inflection line (in the red region), steps follow the direction associated with the negative curvature (associated with lowest eigenvalue of the hessian), while relaxing in the perpendicular direction until a first-order saddle point is found (large black dot in the red region). **2(b)** Once at the saddle point, the system is pushed along  $+\hat{e}_m$  and  $-\hat{e}_m$  to escape the zone where the forces are null (blue arrows) and relaxed toward the adjacent minima (black arrows). Top figures: 3D plot three dimensional landscape. Bottom figures: 2D plot of two-dimension projection of the path; the small black lines are the iso-value levels lines for which the energy is the same. .

relaxation (numerical accuracy) is in general not recommended, because it might lead to the undesired exploration of soft valleys often associated with large elastic deformation.

2. Above the inflection, an orthogonal relaxation is essential to reach the actual valley in which  $F_{\perp}$ , the component of the forces that is orthogonal to  $\hat{e}_m$ , is by definition null. To reduce its computational cost, this relaxation can be stopped when  $F_{\perp}$  becomes smaller than the parallel component  $F_{\parallel}$  by controlling its convergence threshold. However, if the system is not significantly above the inflection, it might happen that this relaxation brings the algorithm back below the inflection, meaning that the lowest mode becomes positive and is associated with elastic deformation, leading to an unsuccessful event. To mitigate the number of unsuccessful searches, ARTn follows a 3-fold strategy by using: (i) non-zero inflection threshold (below  $-0.5 \text{ eV \AA}^2$ ) to determine the point where the system is first above the inflection; (ii) a progressive number of relaxation steps: small close to the inflection and progressively larger; (iii) a smooth switch of the uphill push direction from the initial to the lowest-curvature eigenvector  $\hat{e}_m$  [16].

### 2.5. Reaching adjacent minimum and checking the existence of a connected path

Once the saddle point — defined as a point where  $\lambda_m < 0$  and the total force is below a threshold near zero — has been reached, an adjacent minimum can be found through standard energy minimization, completing the event.

Since forces are zero at the saddle point, a push along the direction of the eigenvector  $\hat{e}_m$  is applied before starting a standard unconstrained minimization to reach the adjacent minimum. This push must be large enough to ensure that the forces are sufficiently large. Applying the push along the opposite direction allows to check the existence of a connected path between the two minima (blue arrows in Fig. 2(b)).

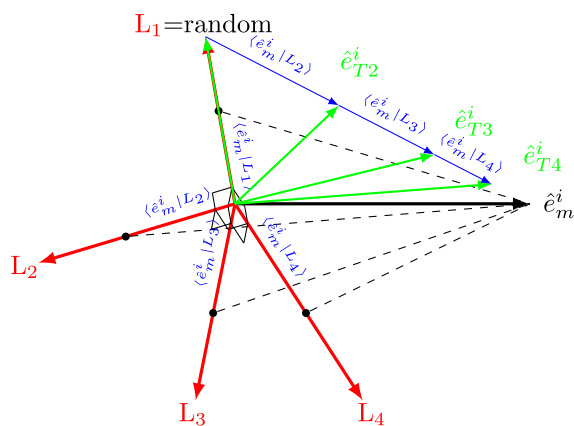
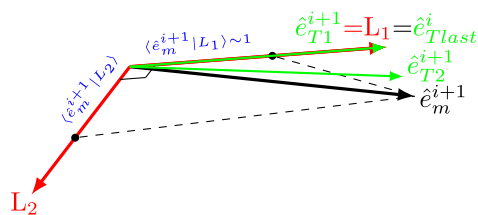
### 3. Improvement of the ARTn core: reducing the number of Lanczos iterations

The computation of the local curvature and associated eigenvectors represents the dominant computational cost for ARTn. This section presents recent developments focused on reducing this cost and improving ARTn's overall computational efficiency.

We refer the reader to a comparative benchmark of the efficiency of ARTn against other existing methods published recently by the authors to complement the benchmarks shown here (see Ref. [16]).

A Lanczos chain starts with a guess basis vector  $L_1$  (see Appendix B) for iteratively determining  $\hat{e}_m$ . This vector can be selected as random or based on informed knowledge. As the ARTn kernel calls the Lanczos algorithm after each push-relax, the eigenvector  $\hat{e}_m^{i+1}$  calculated at the ARTn step  $i+1$  is generally close to the one calculated at the previous step  $i$ . Therefore, if for the Lanczos of the initial ARTn step, the first basis vector  $L_1$  is generated at random, the  $\hat{e}_m^i$  obtained as a result of the Lanczos chain at ARTn step  $i$  can be used as the basis vector  $L_1$  at ARTn step  $i+1$  ( $L_1^{i+1} = \hat{e}_m^i$ ). Indeed, in our experience, the dot product between two consecutive eigenvectors  $\hat{e}_m^i \cdot \hat{e}_m^{i+1}$  is usually lower than 0.7 below the inflection line and higher than 0.95 above it, making the use of the previously converged eigenvector more efficient in this second case (see Fig. 4). Moreover, in this region, the lowest eigenvalue is negative above the inflection, opening up a gap in the spectrum between the first and second lowest eigenvalues. This decreases the mixing of eigenvectors with neighbouring eigenvalues and increases the ratio  $\lambda_i/\lambda_m$  (see Appendix B, Eq. (B.2)).

This means that, using an  $L_1$  close to the eigenvector associated with the lowest curvature, in most cases, convergence can be obtained with a small tridiagonal matrix, as represented in Fig. 3. Since force calculations are much costlier than matrix diagonalization, we implement an adaptive approach where, instead of keeping the Lanczos basis set fixed, as in previous versions of ARTn, the size of the basis is

(a) Lanczos method at ARTn step  $i$ (b) Lanczos method at ARTn step  $i + 1$ 

**Fig. 3.** Scheme of two consecutive Lanczos procedures: one at ARTn step  $i$  and the second at ARTn step  $i + 1$ . The starting Lanczos vector  $L_1$  is random at ARTn step 0 and is the previously converged at ARTn step  $i + 1$ , which implies that fewer Lanczos vectors are needed to converge to  $\hat{e}_m$  at step  $i + 1$ . Each vector is the 2D projection of a  $3N_s D$  vector. The blue brackets  $\langle \hat{e}_m | L_i \rangle$  indicate the projection of the unknown  $\hat{e}_m$  on each of the Lanczos basis vectors  $L_k$ . The previous algorithm was always using 16 Lanczos basis vectors.

progressively increased (see Appendix B) until the lowest eigenvalue reaches convergence (currently set to  $|\frac{\lambda_{mk} - \lambda_{mk-1}}{\lambda_{mk}}| < 10^{-2} \text{ eV/\AA}^2$ ).

In most cases, this iterative approach leads to a significant reduction in the number of force calls associated with the Lanczos procedure with respect to the previous version of the code, despite its former use of the smart starting  $L_1$ . For the systems presented in the next section, for example, this number of force evaluations needed to converge the eigenvector is reduced from 16 (old version) to typically less than 10 below the inflection and less than 5 above the inflection (see black circles Fig. 4), since successive vectors are more parallel.

#### 4. Pre-processing strategies: smart initial pushes

As mentioned previously, ARTn has been applied with success to many systems with a ranging level of complexity and nature. The reader is invited to look at these works for more details. In the following, we focus our attention on two simple examples on which pre-processing strategies can reduce even more the computational cost. In these examples, ARTn is coupled with the *ab initio* software Quantum Espresso v7.0 [23] for the evaluation of energies and forces. ARTn can be used with any other quantum mechanical code, including SIESTA [5], BigDFT [24,25] and VASP [9], as well any continuously derivable empirical potential.

##### 4.1. Diffusion of Al adatom on Al(100) surface

In this first example, we look at the diffusion of an Al adatom on an Al (100) surface, a well studied system with empirical potentials [18].

This example shows how to adopt an event search strategy with minimum bias, in order to reduce the computational cost of the search without affecting the richness of results.

This system is known to be associated with non-intuitive diffusion mechanisms, so called exchange mechanisms, in addition to the simple hopping from adsorption site to adsorption site on the Al(100) surface [18,26]. These exchange mechanisms occur when the adatom takes the place of its first neighbour, which becomes the new adatom or pushes the second (3rd, or 4th) to the surface. These two sets of mechanisms are respectively represented by red (hopping) and black (exchange) arrows in Fig. 5. For a full description of all the possible exchanges, see Fig. 8 of Ref. [18].

If the input vectors are completely random, then half of them shift the adatom in a direction that is opposite to the surface. In these cases, we can easily predict that all the ARTn searches would lead to the dissociation of the adatom from the surface, a physically important mechanism which is of little interest, however, if we are interested in diffusion. To avoid this event, it is possible to restrict the choices of the input vector. In this specific example, we reduce the displacement of the adatom so that it is oriented towards the surface, and restricted to only a quarter of the space since it is symmetrically equivalent to the others.

This constraint is obtained by adding a condition that accepts the random input vector only if the displacement of the adatom is in a cone for which the user gives the direction (11-1) and the half angle ( $45^\circ$ ), as presented Fig. 5. The push on this atom remains random, to preserve the exhaustiveness, but restricted, to save computational cost. This approach can be used on a single atom or generalized to a region, when appropriate.

The PES is calculated using a 300+1 atoms supercell of crystalline aluminium composed by  $5 \times 5$  atoms along the surface, six bulk layers for which the two bottom layers are fixed at the interatomic distance (5.30 Å) and a 18 Å vacuum on top of the surface. The  $\Gamma$  centred sampling of the supercell Brillouin zone is  $2 \times 2$  along the reciprocal surface directions, and an energy cutoff of 15 Ry limits the number of plane waves used to describe the wavefunctions. All explorations of the PES are run in parallel using four different directions simultaneously, with each exploration also taking advantage of the k-point and FFT parallelism capabilities of the DFT software. The total number of explorations is stopped when 50 saddle points are found, as the existence of only about ten low energy saddle points is an *a posteriori* knowledge. All the atoms in the first layer of the surface are taken into account in the initial random displacement.

In this work, ARTn is able to recover all previously identified diffusion mechanisms without their previous knowledge: events with saddle point energies lower than 1 eV are described in Table given in Fig. 5. Each generated events requires on average 170 force calls. Note that our DFT energy barriers are different than the ones that had been obtained with an empirical potential [18], but are similar as the ones previously obtained within DFT: 0.20 and 0.65 eV [26] respectively for the 1st neighbour exchange (Id 1) and the hopping (Id 2).

##### 4.2. Chemical reaction in the gas phase

In this second example, a  $\text{CH}_3\text{Cl}$  molecule is close enough to another Cl atom to form the well known  $\text{Cl}^{\cdot}\dots\text{CH}_3\text{Cl}$  complex [27] shown in Fig. 6(a). From this configuration, the  $\text{CH}_3$  can reverse to catch this  $\text{Cl}^{\cdot}$  while breaking its bond with the other Cl, thus forming the reversed  $\text{ClCH}_3\dots\text{Cl}^{\cdot}$  complex shown in Fig. 6(c). To compute the energy barrier of this reaction, the system is placed in a large unit cell with 15 Å of vacuum in the three directions (to reduce image-image interactions, as Quantum ESPRESSO uses periodic boundary conditions). The position of the Cl atom initially bonded to  $\text{CH}_3$  is kept fixed throughout the procedure to avoid translation of the system, while all the other atoms are allowed to move, fixing the coordinates of an atom not involved in the event has no impact on the result. The push size used to escape the

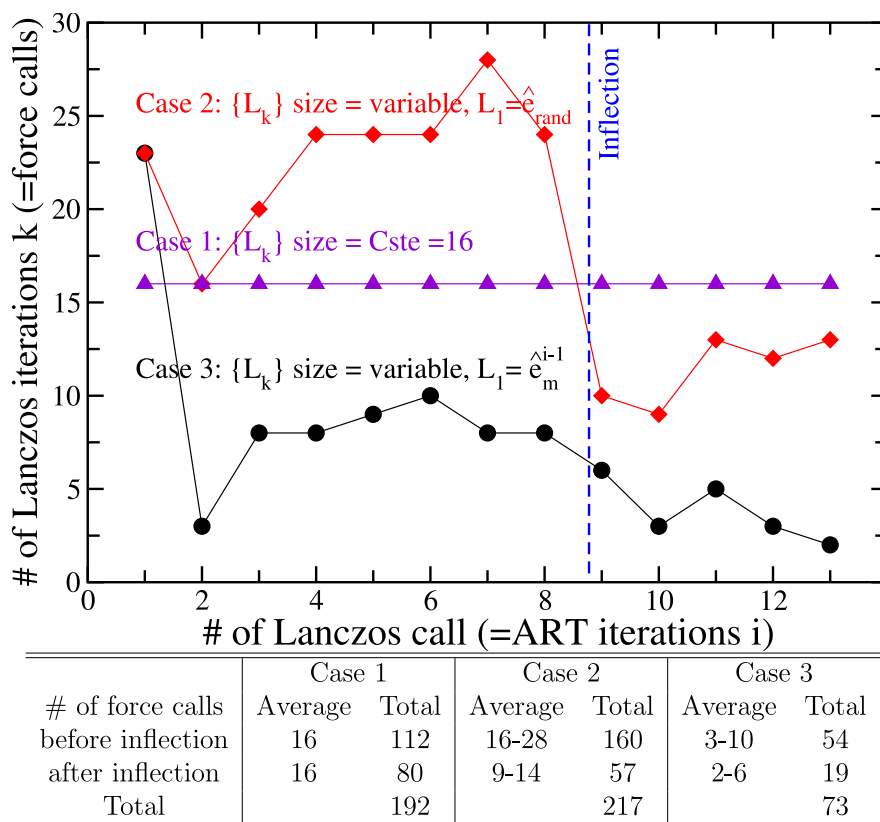


Fig. 4. Typical number of Lanczos iterations (number of force calls) at each new call of the Lanczos algorithm by ART in three different cases. First case (violet triangles): when the size of the Lanczos basis is fixed. Second case (red diamonds): when the size of the Lanczos basis is not predetermined and randomly initialized. Third case (black circles): same as second case but the Lanczos basis is initialized with the previously converged eigenvector ( $L_1^{i+1} = \hat{e}_m^i$ ).

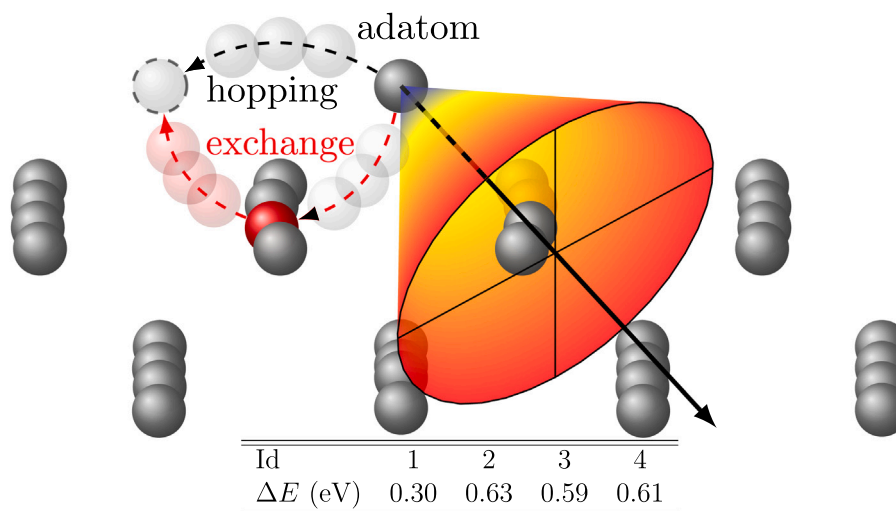


Fig. 5. Top figure: The two first layers of the Al (100) surface and the Al adatom. The cone is centred on the adatom, with the direction  $\langle 11\bar{1} \rangle$  and a  $45^\circ$  angle. An input vector  $\hat{e}_{rand}$  is accepted only if its displacement of the Al adatom is located into this cone. The two possible diffusion mechanisms are shown by the black (hopping — Event Id 2) and red (exchange — Event Id 1) arrows. Bottom table: Transition energies  $\Delta E$  for diffusion events found with a barrier lower than 1 eV. The Id of each event is the same as the ones used in Fig. 8 of Ref. [18]: Id 1, 4 and 3 respectively for the exchange with the 1rst, 3rd and 2nd neighbour, and Id 2 for the hopping. Many other barriers lower than 1 eV have been found around 0.90 eV, but they do not correspond to a diffusion of the adatom, such as the creation of a second adatom or of a vacancy.

area below the inflection is  $0.2 \text{ \AA}$ , which is also the maximum push size above the inflection, the convergence condition on the forces used to define a saddle point is  $0.05 \text{ eV/\AA}$ .

We compare here four pre-processing procedures applied to ARTn in order to recover the saddle point structure detailed in Fig. 6(b). Its energy calculated in this work is  $0.74 \text{ eV}$  which is thus the activation

barrier of this chemical reaction. The basic ARTn-DFT approach corresponds to procedure #1. Procedures #2 to #4 implement additional constraints based on the knowledge of the system that save computational time by reducing the number of force calculations. The number of force calls for each of them is presented in the Table given in Fig. 6.

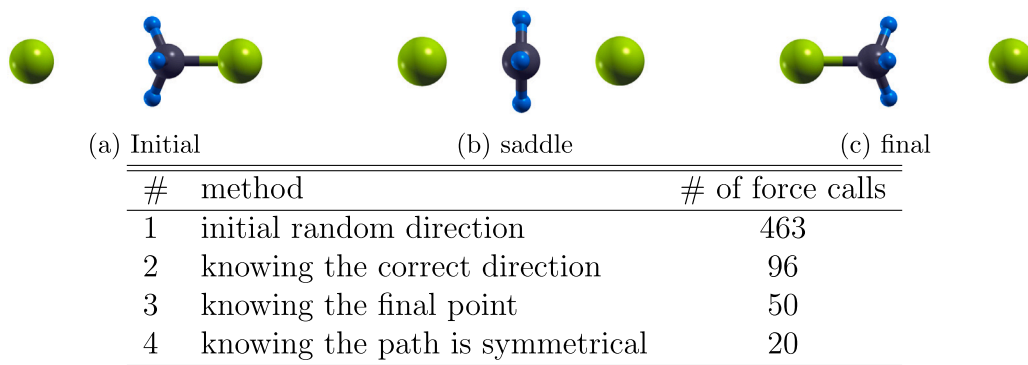


Fig. 6. Top: Atomic structures of the reactants, transition state and products of the chemical reaction of  $\text{CH}_3\text{Cl}$  with a Cl atom. Below: Total number of force calls to find the saddle point for the above reaction using each of the four procedures described in the text. This number of force calls does not take into account the relaxation to the adjacent minimum, which is the same for all.

**Procedure #1:** The only information used is that of the initial position. To generate the desired mechanism, the PES must therefore be explored following the standard unbiased ARTn algorithm shown in Fig. 1, generating different events resulting from each initial random displacement. Here, ARTn generates four different physically-relevant events for this system, for a total of 463 force calls. These events include the separation of one hydrogen atom from the carbon atom (not shown) and the binding transfer from one Cl to the other that we are looking for.

**Procedure #2:** It requires the knowledge of the general direction to the saddle point, which restricts the event search, in a similar spirit to the first example. Instead of launching searches in many random directions and waiting for the desired event to be generated, a specific displacement is directly inputted as the starting deformation: the carbon atom is moved in the exact direction of the isolated Cl. By reducing the number of events searches, this procedure drastically reduces the cost to 96 force calculations, as the algorithm only needs to be run once to find the correct saddle.

**Procedure #3:** It requires the knowledge of the final products of the reaction, which corresponds to a common case in chemistry. With this information, a guessed path can be constructed between the known reactant and the product. ARTn can then start with a structure that is an interpolation between the initial and final structures, which is usually already above the inflection line and close to the saddle point. Here, convergence to the saddle point is obtained in only 50 force evaluations, which is two times less than in procedure #2 and almost 10 times less than in procedure #1. This procedure is also known as r-ARTn [16] and was suggested as an alternative to the computationally expensive string methods.

**Procedure #4:** It requires the knowledge that the path is fully symmetrical. This is not true in general, but is sometimes the case for diffusion in crystalline system, catalysis and simple molecular reactions. Let  $C$  represent the point at the symmetric centre on the diffusion path.  $C$  is known and can be computed for example as  $C = (x_{max}^i + x_{max}^f)/2$ , where  $x_{max}^{i(f)}$  is the triplet of initial (final) coordinates  $(x, y, z)$  of the atom that have the maximal displacement, here the carbon atom. This symmetry implies that  $\hat{e}_m$  can be accurately estimated and provided to ARTn as a pre-processing input. Finally, as in procedure #3, the algorithm can start at an interpolated position, which is, by symmetry, exactly in the centre between the two minima,  $\mathbf{X}^{\text{mid}} = (\mathbf{X}^i + \mathbf{X}^f)/2$ . This starting point is located on a ridge that is orthogonal to the valley due to the symmetry. Each atom relaxes on a straight line linking  $C$  with its starting middle position. The direction of this line is  $\mathbf{X}_C^{\text{mid}} = \mathbf{X}^{\text{mid}} - (C, C, \dots, C)$ , and  $\hat{e}_m$  is thus the component of the total displacement vector  $\Delta\mathbf{X} = \mathbf{X}^i - \mathbf{X}^f$  that is orthogonal to this direction:

$$\hat{e}_m = \Delta\mathbf{X} - (\Delta\mathbf{X} \cdot \mathbf{X}_C^{\text{mid}}) \mathbf{X}_C^{\text{mid}} \quad (2)$$

Reaching the saddle point costs less than half the previous price with only 20 force calculations all called by one single perpendicular relaxation.

## 5. Conclusion

This paper presents a fundamental description of ARTn using an original point of view that clearly shows the link between the various steps of ARTn and the evolution of a system on its own potential energy surface. This knowledge was refined over the last few years, leading to various technical improvements that were presented recently [16], but never explicitly detailed and illustrated. The capacity of ARTn to explore the PES at the *ab initio* accuracy is demonstrated on two systems using a version of the code that includes all these latest improvements and that is embedded into Quantum Espresso [23]. These examples show how to make use of prior knowledge of PES to reduce the computational cost of an unbiased exploration and demonstrate the remarkable efficiency of ARTn local approach to characterize diffusion and activated mechanisms in complex environments.

Over the last two decades, ARTn has already been applied with great success to a wide range of complex systems ranging from proteins aggregation to amorphous surfaces reactions or diffusion in glassy materials. It can therefore be applied to any complex materials to look problems such as catalysis, chemical reaction, structural evolution and much more. With these latest improvements, the method now has unsurpassed accuracy and efficiency and is therefore one of the most powerful tools for the investigation and characterization of activated atomic mechanisms. These significant improvements to ARTn are now available with the Quantum Espresso electronic structure relaxation code. In order to help the development and dissemination of ART in the rest of the community, we are currently working on a more portable version of ART that can be plugged into any software capable of calculating energy and forces with DFT or simple empirical potentials. ARTn will then present itself as a valuable alternative tool to the more conventional methods widely used in the atomic scale community today both for single and double-ended problems.

## Declaration of competing interest

The authors declare that they have no known competing financial interests or personal relationships that could have appeared to influence the work reported in this paper.

## Acknowledgements

NM acknowledges partial support from a Discovery Grant by the Natural Sciences and Engineering Research Council of Canada (NSERC). The simulations were performed using HPC resources from CALMIP

(Grant P1555 and P1418) and from GENCI (Grant A0090911942). Some preliminary work was made possible with the generous computer allocation of Calcul Québec and Compute Canada to NM. All the authors are active members of the Multiscale And Multi-Model Approach for Materials In Applied Science consortium (MAMMASMIAS consortium), and acknowledge the efforts of the consortium in fostering scientific collaborations.

### Software availability

ARTn-DFT is available freely upon request to any of the authors, it includes a complete documentation and many examples. The present version is compatible with QE from QE-6.5 to the present QE-7.0, also available freely at <https://www.quantum-esspresso.org>. We are currently developing a plugin version for an easier use, hands on, maintenance and portability for easy integration into a wide range of *ab initio* and empirical codes.

### Appendix A. Few definitions regarding the potential energy surface

We provide here a few definitions for some of the concepts used in this article regarding the potential energy surface. There are largely based on Ref. [28]. For a summarized version, see Table A.1.

- A *first-order saddle point*, represented Fig. A.7(a), is a maximum along one dimension, and a minimum along the other  $3N_{at} - 1$ . This implies that all the first-order derivatives are zero at this point, and all but one of the Hessian eigenvalues are positive,

Table A.1

Properties of the main remarkable regions and points on the potential energy surface.  $\lambda_i$  represents a Hessian eigenvalue.

	1st derivatives	2nd derivatives
Minimum	$\nabla E = 0$	$\forall i \in \llbracket 1, 3N_{at} \rrbracket, \lambda_i > 0$
Saddle point	$\nabla E = 0$	$\exists i \in \llbracket 1, 3N_{at} \rrbracket, \lambda_i < 0$
Inflection	–	$\exists i \in \llbracket 1, 3N_{at} \rrbracket, \lambda_i = 0$
Below-inflection	–	$\forall i \in \llbracket 1, 3N_{at} \rrbracket, \lambda_i > 0$
Above-inflection	–	$\exists i \in \llbracket 1, 3N_{at} \rrbracket, \lambda_i < 0$
Valley	$\nabla E_{\perp \hat{e}_m} = 0$	–
Ridge	$\nabla E_{\parallel \hat{e}_m} = 0$	–

not counting the trivial macroscopic rotation and translation degrees of freedom. Physically, they are unstable structures that correspond to transition states.

- The *inflection line*, represented by the blue lines Fig. A.7(c), is the set of points for which the smallest eigenvalue of the Hessian is zero.
- The configuration space *below the inflection*, represented in blue Fig. A.7(c), is the space in which all the Hessian eigenvalues are positive: this is where the minima (represented Fig. A.7(a)) are located and where the valleys and ridges begin. When no minima is present, it is a *shoulder*. Its complementary part is the configuration space *above the inflection*, in which at least one Hessian eigenvalue is negative.
- The *valleys*, represented in black Fig. A.7(c), are the set of points for which the gradient is parallel to the eigenvector  $\hat{e}_m$ , i.e. for which the component of the gradient that is orthogonal to  $\hat{e}_m$  is null. This is calculated by splitting the gradient in two components:  $\nabla E = \nabla E_{\perp} + \nabla E_{\parallel}$ , where  $\nabla E_{\perp} = \nabla E - (\nabla E \cdot \hat{e}_m)\hat{e}_m$ . Along the valley, the points of highest energy are the saddle points.
- The *ridges*, represented in white Fig. A.7(c), are the set of points for which the gradient is orthogonal to the eigenvector  $\hat{e}_m$ , i.e. for which  $\nabla E_{\parallel}$  is null. The ridges cross the valleys at the saddle points and at the minima.
- A *basin*, represented in blue Fig. A.7(b), is a set of atomic positions for which an atomic relaxation moves the system toward a same minimum. This is a global definition contrary to all the others which are local. A basin is surrounded by steep energy rises that generally correspond to the ridges except around the extrema where forbidden crossings occur due to the use of eigenvectors in the ridges definition.

### Appendix B. Lanczos diagonalization

The Lanczos algorithm [21] is a particular case of the Arnoldi algorithm [29] that can be simplified when the matrix to be diagonalized is hermitian. This method can deliver the smallest eigenvalue  $\lambda_m$  and its corresponding eigenvector  $\hat{e}_m$  of a potentially very large matrix through the knowledge of the matrix-vector products. In ARTn, this matrix is the Hessian  $H_{ij} = \frac{\partial^2 E}{\partial x_i \partial x_j}$  with size  $3N_{at} \times 3N_{at}$ .

Knowledge of the full Hessian matrix is not needed, because the algorithm only needs its product with a given vector,  $[H]\mathbf{dL}_k$ , at each step  $k$ , where  $\mathbf{dL}$  is a small displacement vector from a reference position. This product can be obtained in only one force calculation:

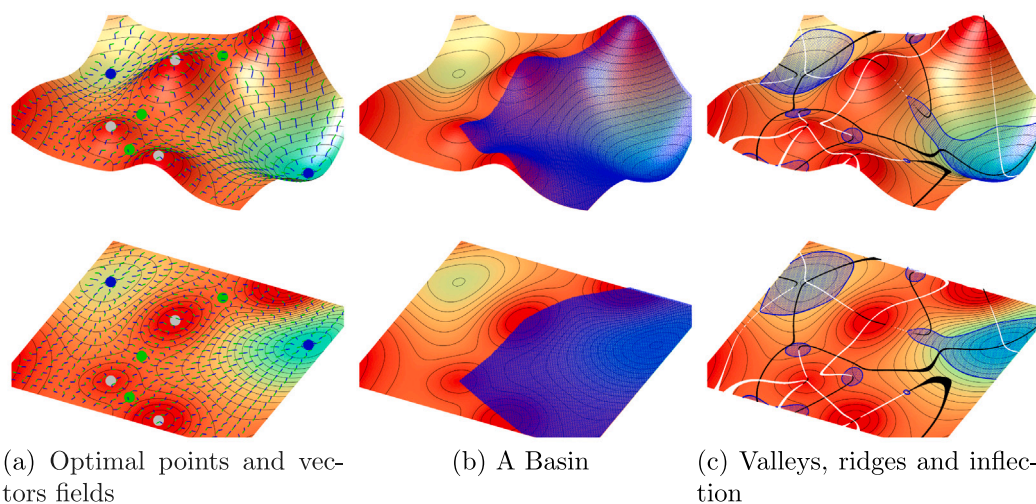


Fig. A.7. Example of a two dimensions PES having A.7(a)- saddle points (green dots), minima (blue dots), maxima (grey dots), a  $\hat{e}_m$  field (green lines pointing towards saddle points), and a force field (blue lines pointing towards minima) A.7(c)- valleys (black lines), ridges (white lines), inflection lines (blue line) surrounding a space below the inflection (blue areas), and A.7(b)- a basin.

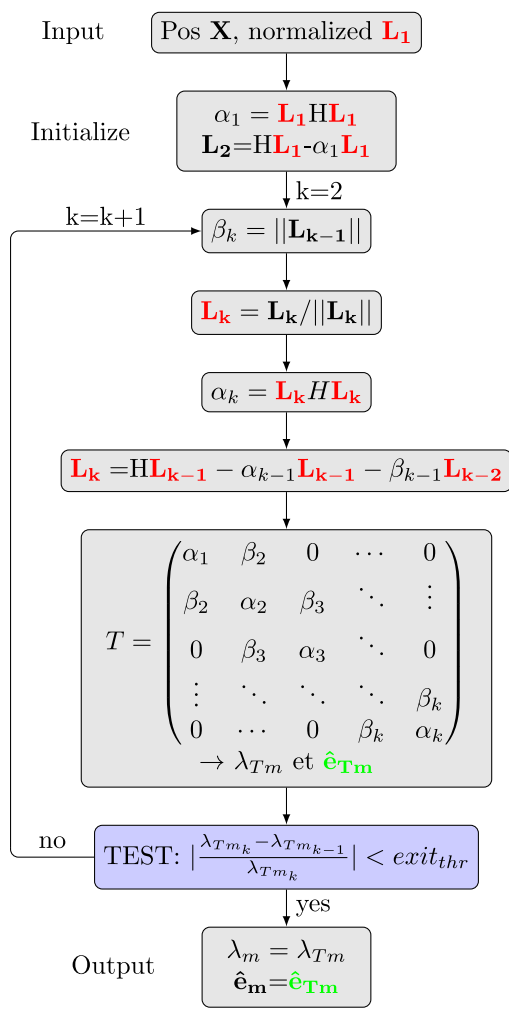


Fig. B.8. Schematic representation of the Lanczos algorithm.

- Do a small distortion  $dr$  of the atomic positions along  $\mathbf{L}$  (forming  $d\mathbf{L}$ ):  
 $\mathbf{X}_{\mathbf{L}} = \mathbf{X} + d\mathbf{L}$
- Calculate the forces at this displaced position with the software (here Quantum Espresso):  
 $\mathbf{F}(\mathbf{X}_{\mathbf{L}}) = -\nabla E(\mathbf{X}_{\mathbf{L}})$
- Return the correct term:  
 $[H]d\mathbf{L} = \Delta\mathbf{F} = \frac{\mathbf{F}(\mathbf{X}_{\mathbf{L}}) - \mathbf{F}(\mathbf{X})}{dr}$ , where  $\mathbf{F}(\mathbf{X})$  has already been calculated in the last minimization step, before entering the Lanczos loop.

To obtain  $\hat{\mathbf{e}}_{\mathbf{m}}$ , the powers method is used. It states that any matrix elevated at a sufficiently high power  $k$  and multiplied by any vector  $\mathbf{L}$  returns an approximation of the eigenvector associated to the highest eigenvalue (lowest for  $-k$ ):

$$\lim_{k \rightarrow +\infty} [H]^{-k} \mathbf{L} = \hat{\mathbf{e}}_{\mathbf{m}} \quad (\text{B.1})$$

It can be simply demonstrated by decomposing  $\mathbf{L}$  on the eigen basis of  $[H]$ , giving  $\mathbf{L} = \sum_{i=1}^{3N_{at}} c_i \hat{\mathbf{e}}_i$  where  $c_1 = c_m$  (minimum), and by factorizing:

$$[H]^{-k} \mathbf{L} = \lambda_m^{-k} c_m \hat{\mathbf{e}}_{\mathbf{m}} + \sum_{i=2}^{3N_{at}} c_i \lambda_i^{-k} \hat{\mathbf{e}}_i \quad (\text{B.2})$$

$$= \lambda_m^{-k} \left( c_m \hat{\mathbf{e}}_{\mathbf{m}} + \underbrace{\sum_{i=2}^{3N_{at}} c_i \left( \frac{\lambda_i}{\lambda_m} \right)^{-k} \hat{\mathbf{e}}_i}_{\rightarrow 0 \text{ as } k \rightarrow +\infty} \right)$$

Here the number of iterations  $k$  needed to converge depends on two conditions :

- The ratio  $\frac{\lambda_i}{\lambda_m}$ . If it is close to one, meaning that  $\lambda_m$  is not separated from the other eigenvalues as it occurs below the inflection, then convergence is slow; on the contrary, if it is close to 0, meaning that  $\lambda_m$  is separated from the other eigenvalues as it occurs above the inflection where one eigenvalue is negative, then convergence is faster.
- The amplitude of the coefficients  $c_{i \neq m}$ . If they are small, this means that the initial vector  $\mathbf{L}$  is already quite converged to  $\hat{\mathbf{e}}_{\mathbf{m}}$ , and less power iterations are needed to achieve the convergence.

With this approach, the algorithm finds an approximate eigenvector, that gets closer and closer to  $\hat{\mathbf{e}}_{\mathbf{m}}$  at each increase of  $k$ . To avoid handling large matrices, it is most cost efficient to use a recurrence scheme :  $\mathbf{L}_{k+1} = [H]\mathbf{L}_k$ , where the initial  $\mathbf{L}_1$  can be random or, better, a reasonable guess for  $\hat{\mathbf{e}}_{\mathbf{m}}$ .

To reduce the number of iterations  $k$  needed to converge to  $\hat{\mathbf{e}}_{\mathbf{m}}$ , Lanczos added two tricks to the power method. First,  $[H]$  is reduced on its subspace generated by the basis of the  $\mathbf{L}_k$  vectors. This is done using a reduction matrix  $[R] = (\mathbf{L}_1 | \mathbf{L}_2 | \dots | \mathbf{L}_k)$ , leading to a tridiagonal matrix  $[T] = [R]^T [H] [R]$ . The size of  $[T]$  is  $k \times k$  and its lowest eigenvalue converges to  $\lambda_{min}$ , because its basis contains more and more parts of  $\hat{\mathbf{e}}_{\mathbf{m}}$ . However the  $\mathbf{L}_k$  basis is not orthogonal. Hence, the second Lanczos idea is to chose each new vector  $\mathbf{L}_k$  such that it is orthogonal to the previous ones by removing their respective contribution:

$$\mathbf{L}_{k+1} = [H]\mathbf{L}_k - \sum_{j=0}^k (\mathbf{L}_{k+1}^T \mathbf{L}_j) \mathbf{L}_j \quad (\text{B.3})$$

These vectors are called the *Lanczos* vectors and contain the part of  $\hat{\mathbf{e}}_{\mathbf{m}}$  coming from the power, but not the parts that are already taken into account in the previous basis vectors. Taking orthogonal vectors means that the next *Lanczos* vector focuses the power method on the components of  $\hat{\mathbf{e}}_{\mathbf{m}}$  that are still unknown, restricting the number of dimensions that still need to be converged.

Thanks to recurrence, this form can be reduce to:

$$\mathbf{L}_{k+1} = [H]\mathbf{L}_k - \alpha_k \mathbf{L}_k - \beta_{k-1} \mathbf{L}_{k-1} \quad (\text{B.4})$$

where

$$\alpha_k = \frac{\mathbf{L}_k^T [H] \mathbf{L}_k}{\mathbf{L}_k^T \mathbf{L}_k} \quad \text{and} \quad \beta_k = \frac{\mathbf{L}_{k-1}^T [H] \mathbf{L}_k}{\mathbf{L}_{k-1}^T \mathbf{L}_{k-1}} \quad (\text{B.5})$$

Finally, the  $[T]$  matrix can be simply written as:

$$T_k = \begin{pmatrix} \alpha_1 & \beta_2 & 0 & \dots & 0 \\ \beta_2 & \alpha_2 & \beta_3 & \ddots & \vdots \\ 0 & \beta_3 & \alpha_3 & \ddots & 0 \\ \vdots & \ddots & \ddots & \ddots & \beta_k \\ 0 & \dots & 0 & \beta_k & \alpha_k \end{pmatrix} \quad (\text{B.6})$$

Upon diagonalization of the matrix  $[T]$ , the lowest eigenvalue  $\lambda_{Tm}$  and its corresponding eigenvector  $\hat{\mathbf{e}}_{Tm}$  are obtained. The eigenvalue  $\lambda_{Tm}$  approximates the lowest eigenvalue  $\lambda_m$  of matrix  $[H]$ , and the corresponding eigenvector  $\hat{\mathbf{e}}_{\mathbf{m}}$  can be constructed from the eigenvector  $\hat{\mathbf{e}}_{Tm}$ , by multiplying  $\hat{\mathbf{e}}_{\mathbf{m}} = [R] \hat{\mathbf{e}}_{Tm}$ . The size of the Lanczos basis (number of iterations  $k$ ) is increased until reaching the convergence criterion, as represented Fig. B.8.

## References

- [1] G.H. Vineyard, Frequency factors and isotope effects in solid state rate processes, *J. Phys. Chem. Sol.* 3 (1957) 121–127, [http://dx.doi.org/10.1016/0022-3697\(57\)90059-8](http://dx.doi.org/10.1016/0022-3697(57)90059-8).
- [2] D.G. Truhlar, B.C. Garrett, S. Klippenstein, Current status of transition-state theory, *J. Phys. Chem.* 100 (31) (1996) 12771–12800, <http://dx.doi.org/10.1021/jp953748q>.
- [3] G.T. Barkema, N. Mousseau, Event-based relaxation of continuous disordered systems, *Phys. Rev. Lett.* 77 (21) (1996) 4358–4361, <http://dx.doi.org/10.1103/PhysRevLett.77.4358>.
- [4] R. Malek, N. Mousseau, Dynamics of lennard-jones clusters: A characterization of the activation-relaxation technique, *Phys. Rev. E* 62 (2000) 7723–7728, <http://dx.doi.org/10.1103/PhysRevE.62.7723>.
- [5] F. El-Mellouhi, N. Mousseau, P. Ordejón, Sampling the diffusion paths of a neutral vacancy in silicon with quantum mechanical calculations, *Phys. Rev. B* 70 (2004) 205205, <http://dx.doi.org/10.1103/PhysRevB.70.205202>.
- [6] S. Santini, N. Mousseau, P. Derreumaux, In silico assembly of alzheimer's  $\alpha$  16-22 peptide into  $\beta$  -sheets, *J. Am. Ceram. Soc.* 126 (37) (2004) 11509–11516, <http://dx.doi.org/10.1021/ja047286i>.
- [7] J.-F. St-Pierre, N. Mousseau, P. Derreumaux, The complex folding pathways of protein A suggest a multiple-funnelled energy landscape, *J. Chem. Phys.* 128 (4) (2008) 045101, <http://dx.doi.org/10.1063/1.2812562>, URL <http://scitation.aip.org/content/aip/journal/jcp/128/4/10.1063/1.2812562>.
- [8] H. Kallel, N. Mousseau, F. Schiettekatte, Evolution of the potential-energy surface of amorphous silicon, *Phys. Rev. Lett.* 105 (4) (2010) 045503, <http://dx.doi.org/10.1103/PhysRevLett.105.045503>.
- [9] N. Salles, N. Richard, N. Mousseau, A. Hemeryck, Strain-driven diffusion process during silicon oxidation investigated by coupling density functional theory and activation relaxation technique, *J. Chem. Phys.* 147 (2017) 054701, <http://dx.doi.org/10.1063/1.4996206>.
- [10] F. El-Mellouhi, N. Mousseau, L. Lewis, Kinetic activation-relaxation technique: An off-lattice self-learning kinetic Monte Carlo algorithm, *Phys. Rev. B* 78 (2008) 153202, <http://dx.doi.org/10.1103/PhysRevB.78.153202>.
- [11] L. Béland, P. Brommer, F. El-Mellouhi, J. Joly, N. Mousseau, Kinetic activation-relaxation technique, *Phys. Rev. E* 84 (2011) 046704, <http://dx.doi.org/10.1103/PhysRevE.84.046704>.
- [12] M. Trochet, L. Beland, J. Joy, P. Brommer, N. Mousseau, Diffusion of point defects in crystalline silicon using the kinetic activation-relaxation technique method, *Phys. Rev. B* 91 (2015) 224106, <http://dx.doi.org/10.1103/PhysRevB.91.224106>.
- [13] A. Jay, M. Raine, N. Richard, N. Mousseau, V. Goiffon, A. Hémercyck, P. Magnan, Simulation of single particle displacement damage in silicon—Part II: Generation and long-time relaxation of damage structure, *IEEE Trans. Nucl. Sci.* 64 (2017) 141–148, <http://dx.doi.org/10.1109/TNS.2016.2628089>.
- [14] S. Mahmoud, N. Mousseau, Long-time point defect diffusion in ordered nickel-based binary alloys: How small kinetic differences can lead to completely long-time structural evolution, *Materialia* 4 (2018) 575–584, <http://dx.doi.org/10.1016/j.mta.2018.11.013>.
- [15] O.A. Restrepo, C.S. Becquart, F. El-Mellouhi, O. Bouhali, N. Mousseau, Diffusion mechanisms of C in 100, 110 and 111 Fe surfaces studied using kinetic activation-relaxation technique, *Acta Mater.* 136 (2017) 303–314, <http://dx.doi.org/10.1016/j.actamat.2017.07.009>.
- [16] A. Jay, C. Huet, N. Salles, M. Gunde, L. Martin-Samos, N. Richard, G. Landa, V. Goiffon, S. De Gironcoli, A. Hémercyck, N. Mousseau, Finding reaction pathways and transition states: r-ARTn and d-ARTn as an efficient and versatile alternative to string approaches, *J. Chem. Theory Comput.* 16 (2020) 6726–6734, <http://dx.doi.org/10.1021/acs.jctc.0c00541>.
- [17] G. Henkelman, B.P. Uberuaga, H. Jonsson, A climbing image nudged elastic band method for finding saddle points and minimum energy paths, *J. Chem. Phys.* 113 (2000) 9901, <http://dx.doi.org/10.1063/1.1329672>.
- [18] G. Henkelman, H. Jónsson, A dimer method for finding saddle points on high dimensional potential surfaces using only first derivatives, *J. Chem. Phys.* 111 (1999) 7010, <http://dx.doi.org/10.1063/1.480097>.
- [19] N. Mousseau, E. Machado-Charry, L.K. Béland, D. Caliste, L. Genovese, T. Deutsch, P. Pochet, Optimized energy landscape exploration using the ab initio based activation-relaxation technique, *J. Chem. Phys.* 135 (3) (2011) 034102, <http://dx.doi.org/10.1063/1.3609924>.
- [20] M.-C. Marinica, F. Willaime, N. Mousseau, Energy landscape of small clusters of self-interstitial dumbbells in iron, *Phys. Rev. B* 83 (9) (2011) 094119, <http://dx.doi.org/10.1103/PhysRevB.83.094119>.
- [21] C. Lanczos, An iteration method for the solution of the eigenvalue problem of linear differential and integral operators, *J. Res. Nat. Bur. St.* 45 (4) (1950) 255–282, <http://dx.doi.org/10.6028/jres.045.026>.
- [22] E. Cancès, F. Legoll, M.-C. Marinica, K. Minoukadeh, F. Willaime, Some improvements of the activation-relaxation technique method for finding transition pathways on potential energy surfaces, *J. Chem. Phys.* 130 (11) (2009) 114711, <http://dx.doi.org/10.1063/1.3088532>.
- [23] P. Giannozzi, S. Baroni, N. Bonini, M. Calandra, R. Car, C. Cavazzoni, D. Ceresoli, G.L. Chiarotti, M. Cococcioni, I. Dabo, A. Dal Corso, S. de Gironcoli, S. Fabris, G. Fratesi, R. Gebauer, U. Gerstmann, C. Gougoussis, A. Kokalj, M. Lazzeri, L. Martin-Samos, N. Marzari, F. Mauri, R. Mazzarello, S. Paolini, A. Pasquarello, L. Paulatto, C. Sbraccia, S. Scandolo, G. Sclauzero, A.P. Seitsonen, A. Smogunov, P. Umari, R.M. Wentzcovitch, QUANTUM ESPRESSO: A modular and open-source software project for quantum simulations of materials, *J. Phys.: Cond. Matter.* 21 (2009) 395502, <http://dx.doi.org/10.1088/0953-8984/21/39/395502>.
- [24] E. Machado-Charry, L.K. Béland, D. Caliste, L. Genovese, T. Deutsch, N. Mousseau, P. Pochet, Optimized energy landscape exploration using the ab initia based activation-relaxation technique, *J. Chem. Phys.* 135 (2011) 034102, <http://dx.doi.org/10.1063/1.3609924>.
- [25] L. Béland, N. Mousseau, Long-time relaxation of ion-bombarded silicon studied with the kinetic activation-relaxation technique: Microscopic description of slow aging in a disordered system, *Phys. Rev. B* 88 (2013) 214201, <http://dx.doi.org/10.1103/PhysRevB.88.214201>.
- [26] P.J. Feibelman, Diffusion path for an Al adatom on Al(001), *Phys. Rev. Lett.* 65 (1990) 729, <http://dx.doi.org/10.1103/PhysRevLett.65.729>.
- [27] G.H. Peslherbe, H. Wang, W.L. Hase, Unimolecular dynamics of Cl ...CH3Cl intermolecular complexes formed by Cl +CH3Cl association, *J. Chem. Phys.* 102 (14) (1995) 5626–5635, <http://dx.doi.org/10.1063/1.469294>.
- [28] A. Lopez, F. Lumberras, J. Serrat, J. Villanueva, Evaluation of methods for ridge and valley detection, *IEEE Trans. Pattern Anal. Mach. Intell.* 21 (4) (1999) 327–335, <http://dx.doi.org/10.1109/34.761263>.
- [29] W.E. Arnoldi, The principle of minimized iterations in the solution of the matrix eigenvalue problem, *Quart. Appl. Math.* 9 (1951) 17–29, <http://dx.doi.org/10.1090/QAM/42792>.